
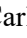

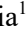

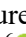

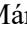


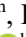


# Swept-source Phase-Stabilized Optical Coherence Tomography Setup for Elastography

Ana Batista<sup>1</sup><sup>a</sup>, Carlos Correia<sup>1</sup><sup>b</sup>, Sílvia Barbeiro<sup>2</sup><sup>c</sup>, João Cardoso<sup>3</sup><sup>d</sup>, José P. Domingues<sup>1,3</sup><sup>e</sup>,  
Rafael Henriques<sup>2</sup><sup>f</sup>, Custódio Loureiro<sup>3</sup><sup>g</sup>, Mário J. Santos<sup>4</sup><sup>h</sup>, Pedro Serranho<sup>1,5</sup><sup>i</sup>,  
Rui Bernardes<sup>1,6</sup><sup>j</sup> and Miguel Morgado<sup>1,3,\*</sup><sup>k</sup>

<sup>1</sup>University of Coimbra, Coimbra Institute for Biomedical Imaging and Translational Research (CIBIT),  
Institute for Nuclear Sciences Applied to Health (ICNAS), Coimbra, Portugal

<sup>2</sup>University of Coimbra, CMUC, Department of Mathematics, Coimbra, Portugal

<sup>3</sup>University of Coimbra, Department of Physics, Faculty of Science and Technology, Coimbra, Portugal

<sup>4</sup>University of Coimbra, Department of Electrical and Computer Engineering, Faculty of Science and Technology,  
Coimbra, Portugal

<sup>5</sup>Universidade Aberta, Mathematics Section, Department of Science and Technology, Lisbon, Portugal

<sup>6</sup>University of Coimbra, Clinical Academic Center of Coimbra (CACC), Faculty of Medicine (FMUC), Coimbra, Portugal


**Keywords:** Optical Coherence Elastography, Swept-source OCT, Phase Stabilization.


**Abstract:** We present an Optical Coherence Elastography (OCE) system, based on a swept-source Optical Coherence Tomography (OCT) setup, and evaluate its performance in terms of phase stability and minimum detectable displacement. The ability to record sub-pixel movements in samples under dynamic conditions was also assessed. The OCE system has a time stability of  $396.9 \pm 46.7$  ps. The phase stability, given by the standard deviation of the measured phase difference, was 72.44 mrad, which corresponds to a minimum detectable displacement of 6.11 nm. Tests showed that the OCE system can detect and measure sub-pixel movements in samples under dynamic mechanical excitation.


## 1 INTRODUCTION


Optical Coherence Elastography (OCE) is a recent imaging modality that maps mechanical properties, by using Optical Coherence Tomography (OCT) to measure tissue displacement after mechanical excitation (Kirby et al., 2017; Larin & Sampson, 2017). Elastography is an inherently highly sensitive technique, since tissue stiffness provides a dynamic


range that can reach six orders of magnitude and OCT has the potential of measuring sub-nanometric displacements. Compared to current clinical elastography techniques, based on ultrasound or magnetic resonance imaging, OCE has the advantage of providing better spatial resolution (1 to 10  $\mu\text{m}$ ), and imaging rate (higher than 1  $\text{kHz}$ ). The main limitation of OCE is its low penetration depth of just a few millimetres (Kennedy et al., 2014). However, this


<sup>a</sup> <https://orcid.org/0000-0002-5672-8266>


<sup>b</sup> <https://orcid.org/0000-0002-2947-1880>


<sup>c</sup> <https://orcid.org/0000-0002-2651-5083>


<sup>d</sup> <https://orcid.org/0000-0002-8832-8208>


<sup>e</sup> <https://orcid.org/0000-0002-0562-8994>


<sup>f</sup> <https://orcid.org/0000-0003-4173-8469>

<sup>g</sup> <https://orcid.org/0000-0001-7856-2124>

<sup>h</sup> <https://orcid.org/0000-0002-0188-7761>

<sup>i</sup> <https://orcid.org/0000-0003-2176-3923>

<sup>j</sup> <https://orcid.org/0000-0002-6677-2754>

<sup>k</sup> <https://orcid.org/0000-0001-9455-1206>

\* Corresponding author

disadvantage is not a limiting factor when imaging ocular tissues.

The high sensitivity of OCE is obtained using phase-sensitive detection techniques. Therefore, OCT instruments for elastography must have a high phase stability, being necessary to minimize the timing jitters and mechanical instabilities and to maximize the signal-to-noise ratio (SNR). Timing jitters are more relevant in swept-source systems than spectrometer-based Fourier-domain setups, because of the frequency jitter introduced by wavelength sweeping based on mechanical moving mirrors (Moon & Chen, 2018).

Several approaches have been implemented to improve phase-stabilisation. Common solutions include using optical timing references, implemented with Mach-Zehnder Interferometers (MZI) optical clocks and Fiber Bragg Gratings (FBG) wavelength-dependent triggers (Moon & Chen, 2018). The MZI provides a clock signal that is periodic in the wavenumber space, usually called k-clock, which is responsible for relative timing. The FBG triggers provide an accurate timing of a given spectral wavelength. Additional reference signals, by setting up a second reference arm, also were proposed (Vakoc et al., 2005). The best results are obtained with a common-path OCT configuration, allowing to measure displacements as low as  $0.3 \text{ nm}$  (Li et al., 2020). However, with a common-path configuration, space compatibility between the setups for mechanical excitation and optical sensing is difficult (Lan et al., 2017). This is particularly true for eye fundus imaging.

Here, we report on our swept-source OCE (SS-OCE) setup and its phase stability. The OCE system was implemented with the purpose of imaging mechanical properties of the retina of mice. Phase stability performance was achieved by using a MZI optical clock and a FBG optical trigger, combined with a novel algorithm for measuring phase-differences (Batista et al., 2022, submitted), and post-processing timing correction using the digitised trigger signal as reference. Tests performed in dynamic conditions, using agarose phantoms that mimic the optical and mechanical properties of biological tissues, showed that the OCE system can detect and measure movements smaller than the axial pixel size, which is around  $320 \text{ nm}$  in our system. Measurements of phase stability resulted in a minimum measurable displacement of  $6.11 \text{ nm}$ .

## 2 SS-OCE SETUP AND DATA ACQUISITION

### 2.1 Instrumentation

Figure 1 presents the schematic of our home-built SS-OCE system. It consists of a swept-source OCT (SS-OCT) and uses, for the dynamic mechanical excitation of the sample, a piezoelectric actuator (P-287, Physik Instrumente GmbH & Co., Karlsruhe, Germany), or a  $10 \text{ MHz}$  ultrasound A-scan probe (Imasonic, Voray sur L'Ognon, France). The SS-OCT is based on a swept-source laser (Axsun, Excelitas Technologies Corp., Mississauga, Canada) emitting at a central wavelength of  $1060 \text{ nm}$ , with a bandwidth of  $110 \text{ nm}$  and a repetition rate of  $100 \text{ kHz}$ . The wavelength sweep is implemented by a tunable MEMS (micro-electromechanical system) filter. The laser source includes a fiber-based MZI to provide a k-clock output, evenly spaced in wavenumber space, for direct analogue-to-digital (A/D) sampling. This makes possible to sample the OCT interferogram linearly in wavenumber, allowing its subsequent direct Fourier processing.

The laser output is split by a 90 to 10 optical fiber coupler, with 90% of the light being used to produce the SS-OCT interferograms and the remaining 10% directed into an FBG (OE Land, Quebec, Canada,  $\lambda_0 = 990 \text{ nm}$ , reflectivity of 99.99%,  $\Delta\lambda = 0.352 \text{ nm}$ ). The FBG is used to produce trigger pulses synchronised with the spectral event corresponding to the Bragg wavelength of  $990 \text{ nm}$  (measured value =  $990.128 \text{ nm}$ ). The optical reflection signal of the FBG, occurring at  $990 \text{ nm}$ , is converted into an electrical signal by a photodiode amplifier and formatted by a digital delay and pulse generator (DG535, Stanford Research Systems, CA, USA).

The light used by the OCT is further split 90:10, respectively, into the sample and reference arms. In the sample arm, the light is delivered and collected from the sample using a 50:50 optical fiber coupler and a long working distance, infinity-corrected, microscope objective (LSM03-BB, Thorlabs Inc., Newton, NJ, USA). The optical setup of the sample arm can be changed when imaging samples containing optical elements, like mice's eyes. In the reference arm, light is reflected from a stationary reference mirror. An in-line fiber optic polarization controller is used to remove differences in polarisation between the sample and reference signals.

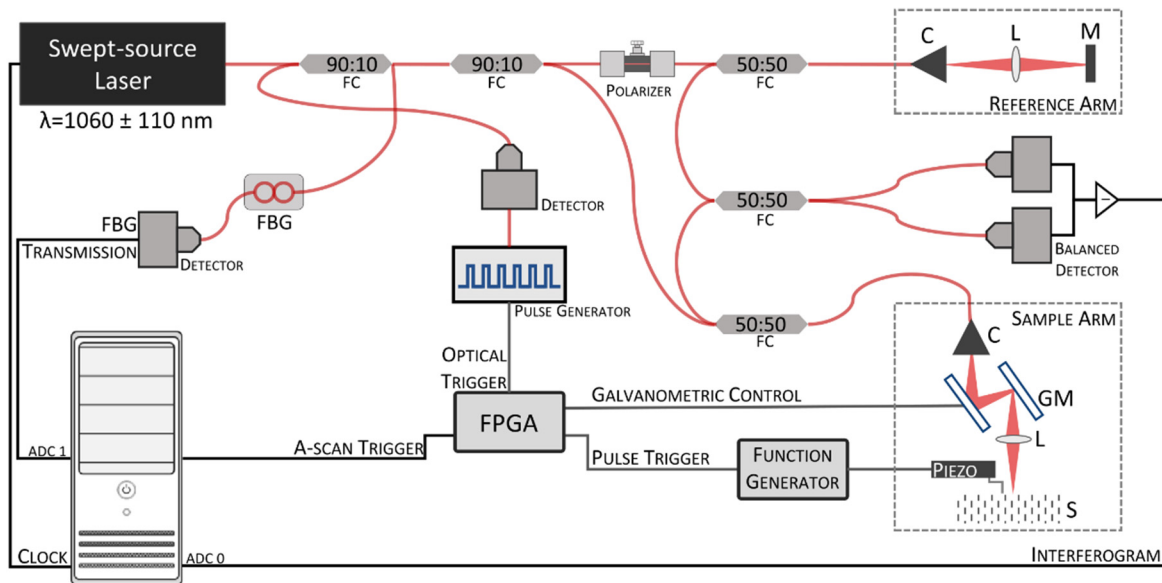


Figure 1: Schematic representation of the SS-OCE system. C – Collimator, L – Lens (microscope objective), M – Mirror, GM – Galvanometric mirrors, ADC – analogue-to-digital converter channel, FC – Fiber Coupler, FBG – Fiber Bragg Grating.

Interference between light coming from the sample and reference arms occurs in a 50:50 optical fiber coupler. The interference fringes are detected by a balanced photodetector (PDB471C, Thorlabs Inc.), which removes common-mode noise. The output of the photodetector is digitised by a data acquisition (DAQ) board (X5-400M, Innovative Integration, Inc., Indianapolis, IN, USA), using the trigger derived from the FBG-generated signal and the laser k-clock output as the sampling clock. Samples are acquired at 400 MHz, with a resolution of 14-bit.

The optical transmission signal from the FBG is also digitised, using the second A/D channel of the DAQ board. This signal is used as timing reference during a post-processing step for additional timing jitter correction. In this step, any shift occurring in the timing reference signal is compensated by shifting the interferogram by an equivalent value. This correction is seldom used, as shifts in the timing reference signal are rare events.

The two-dimensional scanning of the sample is achieved by a pair of galvanometric mirrors (GVS002, Thorlabs, Inc.). Their servo drivers are driven by two 16-bit DACs (LTC2642 from Linear Technology) with a settling time of 1  $\mu$ s, programmed through a 50 MHz SPI interface.

System synchronisation and timing control is the task of a custom-programmed Xilinx XC6SLX45 field-programmable gate array (FPGA). This device receives the trigger from the digital delay generator and produces, with adequate timing, the DAQ board trigger, the transient pulse that triggers mechanical

excitation and the signal that enables galvanometers to move. The FPGA is programmed by the SS-OCE control software running on a PC, through an SPI link provided by an Adafruit FT232H Breakout module.

## 2.2 Control and Acquisition Software

The OCE control software was developed using object-oriented programming (Microsoft Visual C++/IDE) for the 64-bit Microsoft Windows operating system. Libraries from Innovative Technologies were used to deal with data acquisition and DAQ board control.

The software implements the standard OCT acquisition modes: axial A-scan in the sagittal plane, cross-sectional B-scan, in the transversal plane and volumetric acquisition, which can be used to present C-like scans in the coronal plane. Elastography measurements require collecting data using the M-B scanning protocol (Kirby et al., 2017). In this protocol, axial scans are repeated 512 times at a given location. This corresponds to a scanning time of 5.12 ms per location. B-scans are then generated by matching in time several distinct lateral locations. Typically, imaging is performed in 512 distinct lateral positions covering approximately 6.25 mm, in steps of 12.20  $\mu$ m. Sample mechanical excitation occurs once per each lateral location, with a delay of 200  $\mu$ s (corresponding to 20 A-scans) to the beginning of data acquisition for that location.

### 3 DISPLACEMENT CALCULATION

In phase-resolved OCE, the displacement  $\Delta d$  is calculated from the measured phase difference,  $\Delta\phi$ , according to (Kennedy et al., 2014):

$$\Delta d = \Delta\phi \frac{\lambda_0}{4\pi n} \quad (1)$$

where,  $\lambda_0$  is the central wavelength of the laser, and  $n$  is the sample's refractive index.

The phase difference,  $\Delta\phi$ , at each depth  $z$ , is computed as the difference between the phase of two consecutive A-scans ( $\phi_1(z)$  and  $\phi_2(z)$ ), acquired at the same lateral location:

$$\Delta\phi(z) = \phi_2(z) - \phi_1(z). \quad (2)$$

A-scan phases are obtained from the inverse Fourier transform of the interferograms.

We developed a new method to measure phase differences in OCE (Batista et al., 2022, submitted). Briefly, if we consider  $G(k)$  a function in the wavenumber (frequency)  $k$ -space, obtained by concatenating two consecutive interferograms from the same location,  $F_1(k)$  and  $F_2(k)$ , where  $F_1(k)$  is flipped prior to concatenation, its phase ( $\phi_G$ ), given by the angle of its inverse discrete Fourier transform (IDFT),  $g(z)$ , is equivalent to:

$$\phi_G = \phi_{F_2} + \phi_{F_1} + \text{ramp} = \Delta\phi + \text{ramp} \quad (3)$$

where *ramp* corresponds to an amount linearly dependent on depth that ranges from 0 to  $2\pi$  for the entire signal. So, phase differences can be computed directly from the IDFT of the concatenated spectra.

### 4 SYSTEM EVALUATION

Here we present results concerning the timing and phase stability performance of the SS-OCE system and show that the system can detect and measure axial movements smaller than its axial pixel size.

#### 4.1 Time and Phase Stability

For assessing the time and phase stability of our OCE system, we made measurements in static conditions, i.e., without any mechanical excitation, using a gold-coated mirror as sample. Data was recorded with the sample located at the position where the optical path difference between the sample and the reference arm of the OCT interferometer is close to zero, with this position corresponding to the highest signal to noise ratio (SNR).

The system's time stability was assessed by the standard deviation of the interference fringes arrival time at zero-crossing (Li et al., 2020). For finer analysis, we used a cubic interpolation of the data, at zero-crossing, to achieve a time resolution of  $3.5 \text{ ps}$ . Measurements showed that our SS-OCE has a time stability of  $396.9 \pm 46.7 \text{ ps}$ .

The phase stability was assessed by the standard deviation of the measured phase difference ( $\sigma_{\Delta\phi}$ ) in static conditions. Following equation (1), this value can measure the minimum detectable displacement. Figure 2 shows the phase differences over 5000 consecutive interferograms and their distribution. When considering full volumes of 512 M-scans, the distribution of phase differences presents a standard deviation  $\sigma_{\Delta\phi}$  of  $72.44 \text{ mrad}$ , which, according to equation 1, corresponds to a minimum detectable displacement of  $6.11 \text{ nm}$ .

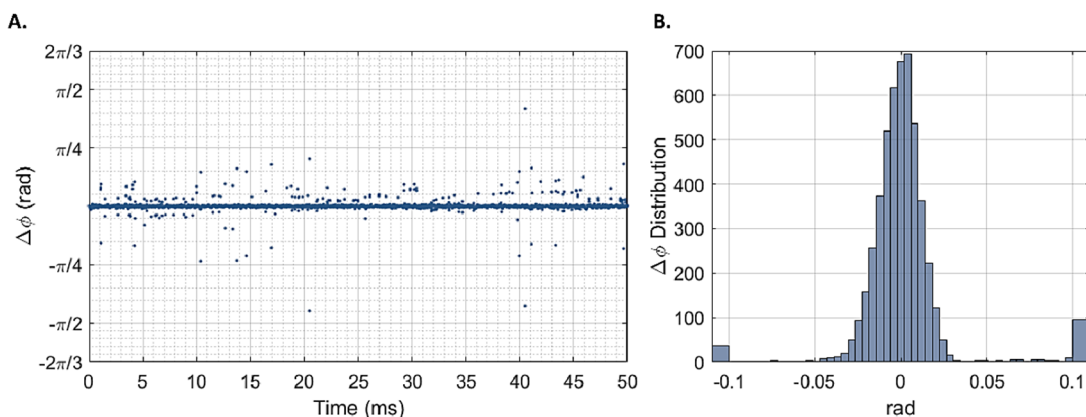


Figure 2: Phase differences ( $\Delta\phi$ ) for a static gold-mirror at highest signal-to-noise ratio, over 5000 consecutive interferograms (A) and their overall distribution (B). This distribution presents a standard deviation  $\sigma_{\Delta\phi}$  equal to  $72.44 \text{ mrad}$ .



## 4.2 Performance in Dynamic Conditions

To assess the performance of the SS-OCE in dynamic conditions, we used transient pulses to induce surface motion in homogeneous agarose phantoms with tissue-mimicking characteristics. These phantoms were prepared by mixing, while stirring, agar with distilled water at high temperature (85°C). Glass microspheres were added to the mixture to increase optical scattering. The mixture was placed into cylindrical containers for moulding and cured for 24 h. The produced phantoms had diameters and heights of approximately 5.2 cm and 3.5 cm, respectively.

The mechanical excitation of the phantoms was provided by the piezoelectric actuator, driven by different pulse widths of 200  $\mu$ s, 300  $\mu$ s, 400  $\mu$ s and 500  $\mu$ s, at a fixed amplitude of 200 mV. These pulses induced, on the surface of the phantoms, displacements lower than the size of the A-scan pixel of the SS-OCT system (around 320 nm). This implies that these displacements were not measurable from the OCT A-scans, which correspond to the plot of the amplitude of the IDFT of the interferograms.

Figure 3 shows the phase difference ( $\Delta\phi$ ) reconstruction for a homogeneous phantom with an agarose concentration of 10 g/l, after mechanical excitation by a transient pulse of 200  $\mu$ s. The figure includes the structural B-scan and  $\Delta\phi$  overlay at 2.56 ms (A), the projection over time for all 512 locations (B) and the  $\Delta\phi$  curves for two locations closer to (d0) and further away (d1) from the excitation point (C). The mechanical excitation was applied approximately 1 mm away from the OCT beam scanning direction (C). From these figures, the SS-OCE system's ability to record sub-pixel displacements is evident.

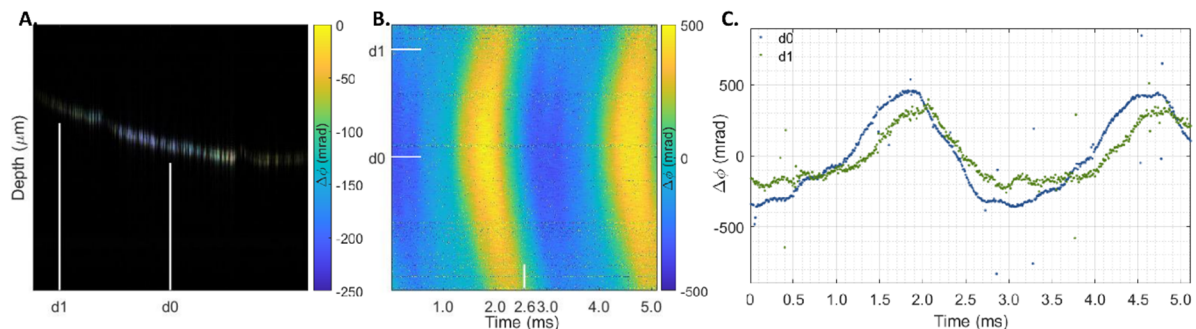


Figure 3: Phase difference ( $\Delta\phi$ ) reconstruction for a 10 g/l homogeneous agarose phantom after a transient pulse of 200  $\mu$ s. Structural B-scan and  $\Delta\phi$  overlay at 2.56 ms (A),  $\Delta\phi$  projection over time (B), and  $\Delta\phi$  curves at two lateral positions located closer (d0) and further (d1) from the piezoelectric actuator contact rod (mechanical excitation), positioned approximately 1 mm away from the OCT beam scanning direction (C). Lateral positions are indicated in the overlay images and projections.

## 5 CONCLUSION

We presented a custom-built, swept-source OCE system, and evaluated its performance under static and dynamic conditions.

The developed SS-OCE presented a time stability of  $396.9 \pm 46.7$  ps. The measured phase stability, given by the standard deviation of the distribution of phase-differences measured in stationary conditions, was 72.44 mrad. This corresponds to a minimum detectable displacement of 6.11 nm.

Tests under dynamic conditions showed that the OCE system can detect and measure sub-pixel movements in samples under dynamic mechanical excitation. The observed phase-differences and, therefore, sample displacements confirm that the system meets the requirements posed by biomedical applications of optical coherence elastography.

The phase stability performance of the OCE system can still be improved. In the shot noise limit, the minimum measurable phase difference corresponds to the reciprocal of the square root of the signal-to-noise ratio (Hyle Park et al., 2005). The phase stability of our system is still one order of magnitude higher than this theoretical limit. One approach to improve the phase performance of the OCE system is to optimize the delays between the timing signals (trigger and clock) and the interferogram. It was shown that signal relative delays have a large impact on phase stabilization due to incoherent timing corrections and collisions between the timing signals (Moon & Chen, 2018). Delay optimization can improve phase stabilization by an order of magnitude, allowing to achieve noise limited performance.

## ACKNOWLEDGEMENTS

This work was financed by FEDER Funds through the Operational Program for Competitiveness Factors - COMPETE and by Portuguese National Funds through FCT-Foundation for Science and Technology under the PTDC/EMD-EMD/32162/2017 project.

Flotte, T., Gregory, K., Puliafito, C. A., Fujimoto, J. G., Izatt, J. A., Kulkarni, M. D., Yazdanfar, S., ... Nelson, J. S. (2005). Phase-resolved optical frequency domain imaging. *Optics Express, Vol. 13, Issue 14, Pp. 5483-5493*, 13(14), 5483–5493. <https://doi.org/10.1364/OPEX.13.005483>

## REFERENCES

- Batista, A., Serranho, P., Santos, M. J., Correia, C., Domingues, J. P., Loureiro, C., Cardoso, J., Barbeiro, S., Morgado, M., & Bernardes, R. (2022). Improving Displacement Measurements in Phase-resolved Optical Coherence Elastography. *Submitted*.
- Hyle Park, B., Pierce, M. C., Cense, B., Yun, S.-H., Mujat, M., Tearney, G. J., Bouma, B. E., de Boer, J. F., Huang, D., Swanson, E., Lin, C., Schuman, J., Stinson, W., Chang, W., Hee, M., Flotte, T., Gregory, K., Puliafito, C., Fujimoto, J., ... Bouma, B. (2005). Real-time fiber-based multi-functional spectral-domain optical coherence tomography at 1.3  $\mu\text{m}$ . *Optics Express, Vol. 13, Issue 11, Pp. 3931-3944*, 13(11), 3931–3944. <https://doi.org/10.1364/OPEX.13.003931>
- Kennedy, B. F., Kennedy, K. M., & Sampson, D. D. (2014). A Review of Optical Coherence Elastography: Fundamentals, Techniques and Prospects. *Ieee Journal of Selected Topics in Quantum Electronics*, 20(2). [doi:10.1109/JSTQE.2013.2268032](https://doi.org/10.1109/JSTQE.2013.2268032)
- Kirby, M. A., Pelivanov, I., Song, S., Ambrozinski, L., Yoon, S. J., Gao, L., Li, D., Shen, T. T., Wang, R. K., & O'Donnell, M. (2017). Optical coherence elastography in ophthalmology. *Journal of Biomedical Optics*, 22(12), 1. <https://doi.org/10.1117/1.JBO.22.12.121720>
- Lan, G., Singh, M., Larin, K. V., & Twa, M. D. (2017). Common-path phase-sensitive optical coherence tomography provides enhanced phase stability and detection sensitivity for dynamic elastography. *Biomedical Optics Express*, 8(11), 5253. <https://doi.org/10.1364/BOE.8.005253>
- Larin, K. V., & Sampson, D. D. (2017). Optical coherence elastography – OCT at work in tissue biomechanics [Invited]. *Biomedical Optics Express*, 8(2), 1172. <https://doi.org/10.1364/BOE.8.001172>
- Li, Y., Moon, S., Chen, J. J., Zhu, Z., & Chen, Z. (2020). Ultrahigh-sensitive optical coherence elastography. *Light: Science & Applications* 2020 9:1, 9(1), 1–10. <https://doi.org/10.1038/s41377-020-0297-9>
- Moon, S., & Chen, Z. (2018). Phase-stability optimization of swept-source optical coherence tomography. *Biomedical Optics Express*, 9(11), 5280. <https://doi.org/10.1364/BOE.9.005280>
- Vakoc, B. J., Yun, S. H., de Boer, J. F., Tearney, G. J., Bouma, B. E., Huang, D., Swanson, E. A., Lin, C. P., Schuman, J. S., Stinson, W. G., Chang, W., Hee, M. R.,